PHYSICAL REVIEW E **95**, 062903 (2017)

Charging changes contact composition in binary sphere packings

André Schella,[1,*] Simon Weis,[2] and Matthias Schröter[1,3]
[1]*Max Planck Institute for Dynamics and Self-Organization Göttingen, 37077 Göttingen, Germany*
[2]*Institute of Theoretical Physics I, University Erlangen-Nürnberg, Staudtstraße 7, 91058 Erlangen, Germany*
[3]*Institute for Multiscale Simulation, Friedrich-Alexander University, 91052 Erlangen, Germany*

(Received 24 March 2017; published 15 June 2017)

Equal volume mixtures of small and large polytetrafluorethylene spheres are shaken in an atmosphere of controlled humidity which allows one to also control their tribocharging. We find that the contact numbers are charge dependent: As the charge density of the beads increases, the number of same-type contacts decreases and the number of opposite-type contacts increases. This change is *not* caused by a global segregation of the sample. Hence, tribocharging can be a way to tune the local composition of a granular material.

DOI: 10.1103/PhysRevE.95.062903

I. INTRODUCTION

The term granular media comprises all ensembles of particles where the individual entities are large enough to be unaffected by Brownian motion. Besides gravity and contact forces, the dynamics of granular media is also controlled by forces originating from the surface of the particles: electrostatic interactions [1], capillary forces [2], and friction [3]. Understanding the role of these forces is not only an interesting scientific problem, but also important for technological applications because many raw materials in industry come in granular form [4]. Especially, tribocharging of granular particles proves to be challenging because it can lead to both repulsive and attractive interactions between the beads [5–10].

The simplest model system to investigate generally polydisperse granular materials are binary sphere mixtures. They have been widely studied with respect to their jamming behavior [11–14], their structural features [15,16], and their binary contact numbers [17–21]. Binary sphere packings agitated vertically tend to segregate [22–27]. Depending on the prevailing segregation mechanism, the larger spheres either rise to the top (which is also called the Brazil nut effect), or they sink to the bottom. Segregation is a common problem in the manufacturing industry where mixing of different types of granular materials is often a crucial process [28–31].

Tribocharging is pervasive in the handling of granular material because every time two materials get in contact, some charge will be transferred [1,32,33]. Tribocharging of granular samples can lead to the formation of clusters [5], demixing [34], or even prevent pore clogging [35]. Recently, we have shown that tribocharging can also be used to counteract segregation [36].

The amount of tribocharging is known to depend on the humidity of the air [36–43]. Here, we use this dependence to control the amount of surface charges on the beads in a binary mixtures of Teflon spheres. At the same time we ensure that the charges are large enough to avoid global segregation. Using x-ray tomography we then investigate how the composition of small-small, small-large, and large-large contacts changes as a function of the surface charge.

II. EXPERIMENT

All experiments are performed with a mixture of approximately 10000 small and 1483 large polytetrafluorethylene (PTFE) spheres, purchased from TIS. The radius of the small spheres r_s is 0.795 mm (±3.1% according to the manufacturer), the large spheres have a radius r_L of 1.5 mm (±0.8%).

The binary mixtures are shaken sinusoidally in cylindrical containers (diameter 50 mm, made of polyamide Nylon 6-6) using an electromagnetic shaker (LDS 406). In order to assure steady state conditions, all samples are shaken for 1 h at a frequency of 100 Hz and an acceleration of 2 g. To avoid the accumulation of dust, the beads and the container are cleaned with ethanol and pure water after each five measurements.

The average charge of individual beads is measured after the shaking has stopped by extracting ten large beads and ten small beads from the sample using an antistatic tweezer. The beads are then deposited into a Faraday cup connected to a Keithley 6514 electrometer. Because the magnitude of the charge on a dielectric particle will scale with the beads' surface area, we consider here the surface charge density $\sigma_{L,s} = Q_{L,s}/4\pi r_{L,s}^2$ of large respectively small beads instead of the total magnitude of charge $Q_{L,s}$ [44]. We note that the sum of all charges on the beads is not necessarily zero, as the walls of the shaking container will also charge electrostatically.

In order to modify the charge accumulation on the beads, the experiments are performed under controlled relative humidity (RH). A self-built climate chamber equipped with a cooling trap and an ultrasonic transducer allows one to tune the ambient humidity in the range between 10% RH and 100% RH [36]. The humidity inside the chamber is logged constantly and changes on average about 2% RH during the course of an experiment. Humidity control is started 1 h prior to the experiment in order to equilibrate the water content on the surface of the beads and the container walls [45].

An advantage of using PTFE beads is their high contact angle with water (108° [46]) which prevents the formation of capillary bridges at high humidity levels. Consequentially, segregation due to capillary attraction [47,48] will not affect our experiments.

Figure 1 demonstrates that under our shaking conditions, large spheres charge negatively and small spheres charge positively. This observation is the opposite of what has been

---

[*] andre.schella@ds.mpg.de

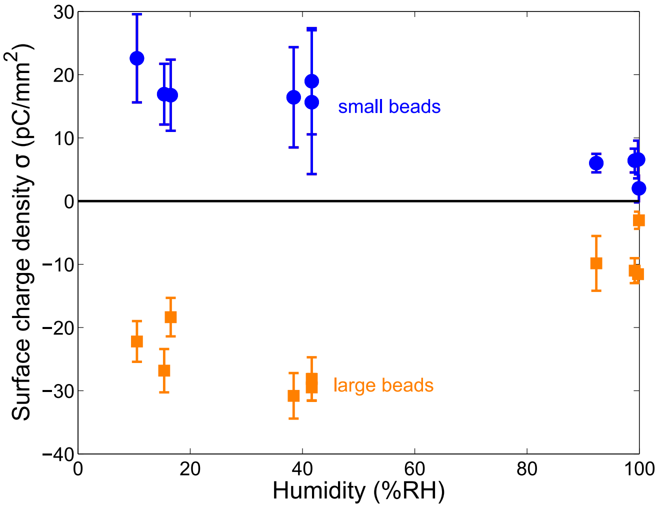

FIG. 1. The amount of charge accumulated by shaken PTFE spheres depends on the relative humidity, and the sign depends on the size of the particles with small particles being positively and large particles being negatively charged. Data are taken from samples of equal volumes of small and large PTFE spheres, shaken vertically in a polyamide container.

found in previous granular experiments [49–51] and predicted by some models of same-material tribocharging [52,53]. A result similar to our observation was found in experiments with spheres sliding along a plane made from the same material [54,55].

To estimate the threshold for tribocharging, we have deionized large PTFE beads on a grounded metal plate using an electrostatic ion gun prior to depositing them in the Faraday cup. The residual charge density on these beads was found to be $\sigma_{\text{th}} = -1.8\ \text{pC/mm}^2$ ($Q_{\text{th}} = -52$ pC), which is comparable to previous results [56].

A. X-ray computed tomography

The structure of the packings created by shaking is analyzed using x-ray computed tomography. The tomography setup (Nanotom, General Electrics) is operated at 130 kV and 90 μA using a tungsten target. The side length of a voxel [which is the three-dimensional (3D) equivalent of a pixel] is 60 μm^3 and data sets consist typically of 900 × 900 voxels in the horizontal direction and, depending on the expansion of the bed, 800–900 voxels in the vertical direction.

Particle centers and radii are identified using the image processing procedure described in Ref. [36]. Since the structural features of the tribocharged mixtures might be modified in the vicinity of the walls [57], we exclude all particles which are closer than three large particle diameters to the container walls from our further analysis. At the top and bottom we discard two layers of large particles. The remaining core region consists of 3090 ± 430 particles.

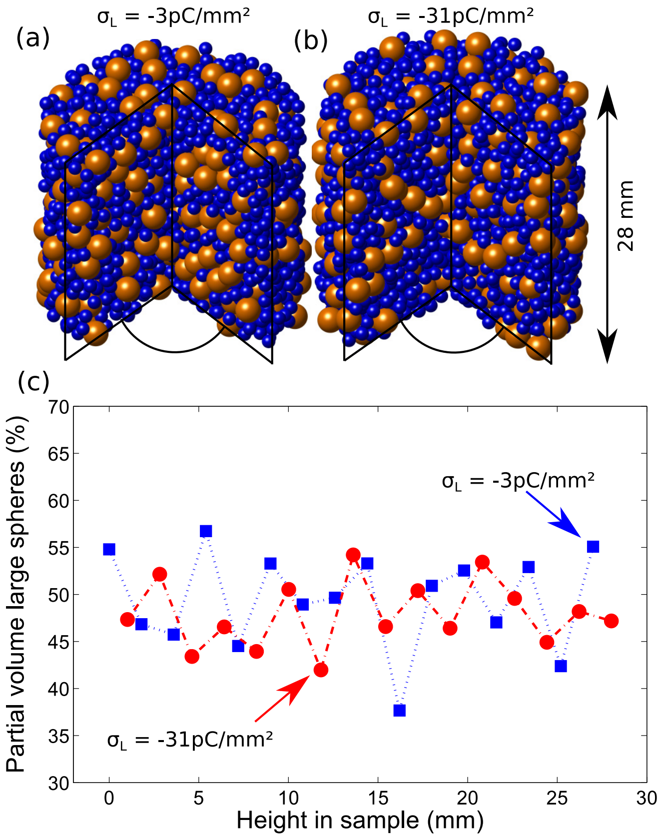

FIG. 2. Renderings of binary packings of small and large PTFE spheres. Particle positions were acquired using x-ray tomography. A 90° wedge has been removed to visualize the interior structure. Both samples have been shaken vertically for 1 h at 2 g, but at different humidity levels. (a) corresponds to the sample with the least charged large spheres and (b) to the one with the strongest charge. Neither sample shows macroscopic segregation, i.e., differences in the vertical distribution of the large spheres with respect to the small ones. This is also shown quantitatively in (c), which displays the height dependence of the volume contributed by the large spheres to the total particle volume for low (blue squares) and high (red circles) charge density.

Figures 2(a) and 2(b) show reconstructed sphere positions from the inner part of two samples, with the two panels corresponding to the samples with the smallest and largest surface charge density on the large spheres. Neither packing shows signs of vertical segregation. This can also be seen in Fig. 2(c): Within fluctuations the contribution of the large spheres to the total volume is one half, independent of height. This result holds also for all other experiments reported here.

The x-ray tomographies allow us to compute both the average number of contacts of the spheres and the volume fraction ϕ of the packing. A binary mixture has four different contact numbers: first, the number of contacts an average large spheres forms with other large spheres Z_{LL}, or with small spheres Z_{Ls}, then, the number of contacts an average small sphere forms with large spheres Z_{sL} (which is different from Z_{Ls}; cf. Sec. III), and finally, the number of contacts between small spheres Z_{ss}. We have measured those four numbers by adapting the contact number scaling function method described in Refs. [58–60]. Details can be found in the Appendix.

In order to compute the volume fraction of the analyzed region, without the interference of any boundaries, we first perform a set Voronoi tessellation of our sample which assigns each point of the interstitial space between the particles to the sphere whose surface is closest [60,61]. The global packing fraction is then computed as

$$\phi = \frac{\frac{4\pi}{3}\left(N_L r_L^3 + N_s r_s^3\right)}{\sum_i^{N_L} v_L^i + \sum_j^{N_s} v_s^j}. \tag{1}$$

The numerator contains the total volume of all the N_L large and N_s small spheres in the analyzed region and the denominator the sum of all the individual Voronoi volumes v_L and v_s of the large respectively small spheres.

III. CHARGE CONTROLS THE CONTACT NUMBERS

Figure 3 shows the main result of our study: The binary contact numbers exhibit a clear dependence on σ_L and σ_s. The numbers of large-small and small-large contacts, Z_{Ls} and Z_{sL}, increase linearly with increasing electrostatic charge density. At the same time the numbers of same-type contacts, Z_{LL} and (less obvious) Z_{ss}, decrease with increasing surface charge density. This change in contact numbers is in good agreement with a simple model assuming that like-charged large beads repel each other whereas oppositely charged particles attract each other.

The increase of opposite-type contacts in charged samples is also compatible with the visual impression gathered from Figs. 2(a) and 2(b). While neither of the two packings shows macroscopic segregation, the local structure differs in that the large particles form more stringlike structures in the highly charged sample. Similar structures have been identified in simulations of charged binary colloidal aggregates [62] and monodisperse charged grains [7]. An interesting follow-up question will be if these changes in microstructure do also alter the macroscopic mechanical behavior of the material. This would open an avenue for granular packings with tunable properties.

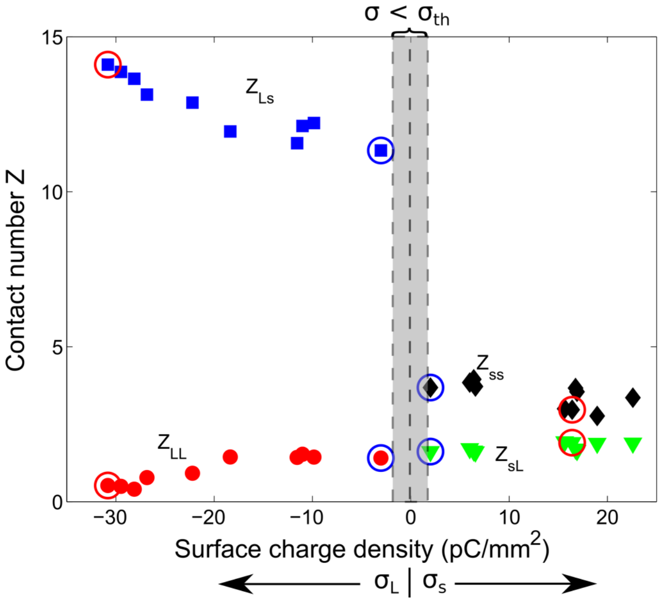

FIG. 3. Number of large-large Z_{LL}, large-small Z_{Ls}, small-large Z_{sL}, and small-small Z_{ss} contacts in a binary mixture as a function of the average surface charge density of the large respectively small beads. Circles identify the two packings depicted in Figs. 2(a) (blue) and 2(b) (red). The shaded region corresponds to the residual charge regime where $|\sigma| < 1.8$ pC/mm^2.

There is a noticeable difference in how strong Z_{Ls} and Z_{sL} depend on their respective σ, i.e., $\partial Z_{Ls}/\partial\sigma_L > \partial Z_{sL}/\partial\sigma_s$. This difference can be explained using the fact that the total number of large-small contacts in a given volume is the same as the number of all small-large contacts, $N_L Z_{Ls} = N_s Z_{sL}$. Taking the derivative with respect to an average σ, we obtain

$$\frac{\partial Z_{Ls}}{\partial\sigma} = \frac{N_s}{N_L}\frac{\partial Z_{sL}}{\partial\sigma}, \tag{2}$$

where we have used the additional condition that the total number of particles in the observation volume is independent of the charge, which is indeed justified in our experiments. As we have studied equal volume mixtures, Eq. (2) predicts $N_s/N_L = (r_L/r_s)^3 \approx 6.7$. A linear fit to the data of Fig. 3 yields $\partial Z_{Ls}/\partial\sigma \approx 5.5\,\partial Z_{sL}/\partial\sigma$, which is in reasonable agreement with the predicted slope ratio.

We can also compare our contact numbers results with previous experimental [18] and theoretical [19,20] work on the contact numbers of uncharged binary mixtures. A linear regression of our data and an extrapolation to the value $\sigma \to 0$ pC/mm^2 yields $Z_{LL} = 1.9$, $Z_{Ls} = 10.9$, $Z_{sL} = 1.6$, and $Z_{ss} = 4$, which agrees well with the previously published results for packings of comparable size ratio.

IV. AVERAGE CONTACT NUMBER AND GLOBAL PACKING FRACTION

In the previous section we have shown that tribocharging leads to a local rearrangement and hence changes the binary contact composition. However, tribocharging does also affect global quantities of the binary sphere packings, as shown in Fig. 4. The packing fraction ϕ decreases approximately 1% with increasing surface charge density. This trend is in agreement with simulations of monodisperse particles [7].

The average contact number $\langle Z\rangle$ does also decrease with increasing surface charge density. Hence, the bed expands and gets looser. Such a correlation of ϕ and $\langle Z\rangle$ is to be expected based on previous studies of monodisperse sphere packings [58,63].

Qualitatively, increasing the charge density on the beads will also increase attractive interactions between large and small particles. Thus, a decreasing packing fraction with increasing charge density seems counterintuitive at first glance. However, attractive interactions also alter the mechanical stability of granular packings since these have a stabilizing effect, causing the formation of chainlike, porous structures [7,62]. To what extent additional many-body [31] or polarization effects of the dielectric beads [5,6,62] contribute to our findings has to be clarified in future studies.

V. SUMMARY

Binary systems of dielectric particles have been shaken vertically at different humidity levels which allows one to control the tribocharging of the beads. Because small and large beads differ in the sign of their charge, the resulting attractive

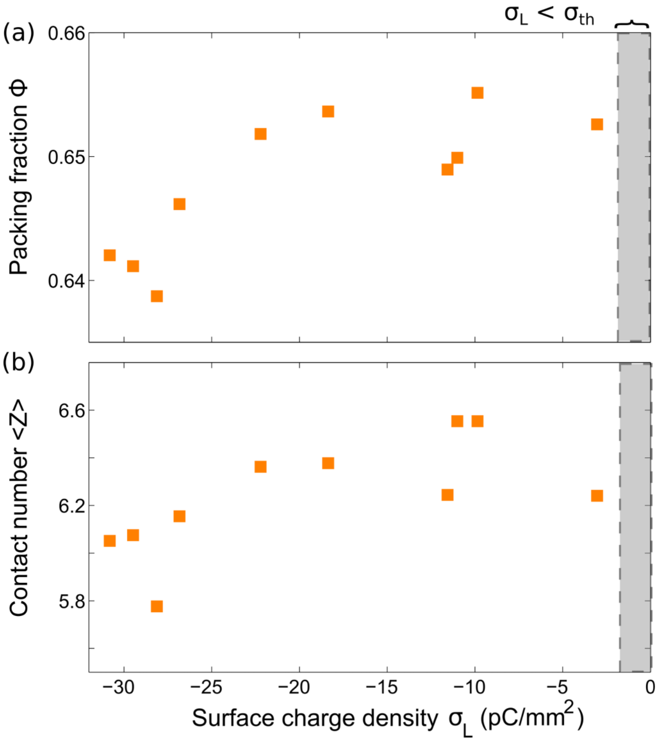

FIG. 4. The global packing fraction ϕ and the average contact number $\langle Z\rangle$ depend weakly on the surface charge density σ_L. The shaded region marks the residual charge regime where $\sigma_L < -\sigma_{\rm th}$.

interactions inhibit macroscopic segregations of the sample. At the same time the electrostatic interactions change the local structure of the packing: The stronger the charge carried by the individual particles is, the more likely becomes the formation of contacts between small and large beads at the expense of same bead-type contacts. Previous studies of binary packings stated that the composition of contacts can be changed by changing the number ratio of small to large particles. Here, we suggest an alternative route: The composition of contacts can also be altered by tribocharging the particles.

ACKNOWLEDGMENT

We thank Wolf Keiderling for repeated mechanical support.

APPENDIX: CONTACT NUMBER ANALYSIS

A contact between bead A and B is defined as touching beads, i.e., when the distance d between the beads is equal to the particle radii $d = r_A + r_B$. Applying this definition to experimental data, as, e.g., gathered by x-ray tomography, is a challenging task due to two reasons. First, errors in the image acquisition and processing add random noise to the particle coordinates and therefore distances between pairs of particles. Second, all granular particles are to some degree polydisperse, hence $r_A + r_B$ is not a constant but depends on the individual particles under consideration. To mitigate these two problems we use an ensemble based fitting method which determines Z_{AB} by modeling the effect of inaccuracies in the particle coordinates using the best average representations of r_A and r_B [58–60].

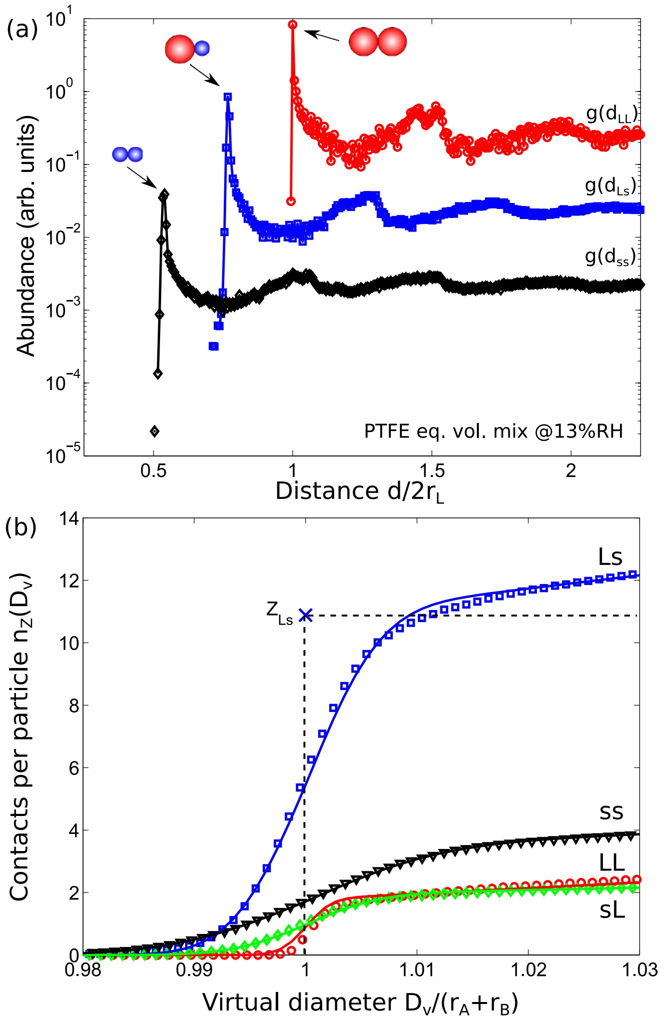

FIG. 5. (a) Binary radial distribution functions $g_{AB}(d)$ of an equal volume mixture of tribocharged PTFE spheres. The position of the first peak provides the best estimates for the three different sums of radii. Functions are shifted vertically for better visibility. (b) In order to account for experimental uncertainties of the detected particle positions, particle radii are scaled up and down and the number of contacts per particle n_Z is counted for the different virtual diameters V_v. Fitting these data with the contact number scaling function Eq. (A3) allows us to measure the three different contact numbers Z_{AB}.

The method works in two steps. First, the average interparticle distance $\langle r_A + r_B\rangle$ is determined from the first peak of the binary radial distribution function $g_{AB}(d)$ which measures the probability to find a particle of type B in a distance d from a given particle of type A. $g_{AB}(d)$ can be computed by counting the number of particles in spherical shells around a reference particle,

$$g_{AB}(d) = \left\langle \frac{1}{4\pi d^2 \rho} \sum_{B,j} \delta(d - |\vec{x}_A - \vec{x}_{B,j}|) \right\rangle_A . \qquad \text{(A1)}$$

Here, the sum over j runs over all particles of type B and the delta function gives only a contribution if the distance between the two particle centers $|\vec{x}_A - \vec{x}_{B,j}|$ is equal to d. The triangular brackets denote the average over all particles of type A. The normalization consists of two parts: The volume of the spherical shell analyzed grows with $4\pi d^2$ and by dividing with the number density ρ we assure that an uncorrelated system will have $g_{AB}(d) = 1$.

Figure 5(a) shows the large-large $g_{LL}(d)$, large-small $g_{Ls}(d)$, and small-small $g_{ss}(d)$ pair distributions for a mixture shaken at approximately 13% RH. The first peak in these distributions originates from particle pairs in contact, therefore an extrapolation of the peak positions provides the best possible estimate for the three different combinations of $\langle r_A + r_B\rangle$.

To determine the four different contact numbers Z_{AB} we follow an adapted version of the procedure described in Refs. [59,60]. First, we determine how the number of contacts $n_{Z_{AB}}$ (defined as touching or overlapping particles) changes if we multiply the particle radii with a scaling factor, thereby creating particles with virtual diameters D_v ranging from 0.98 to 1.03 times $2r_A$ respectively $2r_B$. The resulting $n_{Z_{AB}}(D_v)$ can be seen in Fig. 5(b).

The idea is that errors in the particle positions due to image processing and polydispersity should be Gaussian distributed. We expect therefore that for virtual diameters smaller than $D_{\text{avg}} = \langle r_A + r_B\rangle$ the binary contact numbers n_Z will follow a cumulative normal distribution

$$n_Z(D_v) = \frac{Z_{AB}}{\sqrt{2\pi}\sigma}\int_0^{D_v} \exp\left(-\frac{(D_v' - D_{\text{avg}})^2}{2\sigma^2}\right) dD_v', \quad \text{(A2)}$$

where the experimental uncertainties are captured by the variance σ and Z_{AB} is the average contact number we try to determine.

For $D_v > D_{\text{avg}}$, a linear term has to be added to $n_Z(D_v)$ to account for close, but noncontacting, particles, i.e., particles from the right shoulder of the first peak of $g_{AB}(d)$. The full contact number scaling function is thus given by

$$n_{\text{CNS}}(D_v) = n_Z(D_v) + \Theta(D_v - D_{\text{avg}}) m (D_v - D_{\text{avg}}), \quad \text{(A3)}$$

with m being an unknown slope and Θ the Heaviside function.

Figure 5(b) shows that Eq. (A3) provides reasonable fits for all four possible combinations of binary contacts.

[1] S. Matsusaka, H. Maruyama, T. Matsuyama, and M. Ghadiri, Triboelectric charging of powders: A review, Chem. Eng. Sci. **65**, 5781 (2010).

[2] S. Herminghaus, *Wet Granular Matter: A Truly Complex Fluid* (World Scientific, Singapore, 2013).

[3] M. Schröter, A local view on the role of friction and shape, arXiv:1703.07151.

[4] J. Duran, *Sands, Powders, and Grains* (Springer, New York, 2000).

[5] V. Lee, S. R. Waitukaitis, M. Z. Miskin, and H. M. Jaeger, Direct observation of particle interactions and clustering in charged granular streams, Nat. Phys. **11**, 733 (2015).

[6] J. Qin, J. Li, V. Lee, H. Jaeger, J. J. de Pablo, and K. F. Freed, A theory of interactions between polarizable dielectric spheres, J. Colloid Interface Sci. **469**, 237 (2016).

[7] S. Chen, S. Li, W. Liu, and H. A. Makse, Effect of long-range repulsive Coulomb interactions on packing structure of adhesive particles, Soft Matter **12**, 1836 (2016).

[8] R. Yoshimatsu, N. A. M. Araújo, T. Shinbrot, and H. J. Herrmann, Field driven charging dynamics of a fluidized granular bed, Soft Matter **12**, 6261 (2016).

[9] J. Kolehmainen, A. Ozel, C. M. Boyce, and S. Sundaresan, Triboelectric charging of monodisperse particles in fluidized beds, AIChE J. **63**, 1872 (2017).

[10] R. Yoshimatsu, N. A. M. Araújo, G. Wurm, H. J. Herrmann, and T. Shinbrot, Self-charging of identical grains in the absence of an external field, Sci. Rep. **7**, 39996 (2017).

[11] A. B. Hopkins, Y. Jiao, F. H. Stillinger, and S. Torquato, Phase Diagram and Structural Diversity of the Densest Binary Sphere Packings, Phys. Rev. Lett. **107**, 125501 (2011).

[12] A. B. Hopkins, F. H. Stillinger, and S. Torquato, Disordered strictly jammed binary sphere packings attain an anomalously large range of densities, Phys. Rev. E **88**, 022205 (2013).

[13] D. Chen and S. Torquato, Confined disordered strictly jammed binary sphere packings, Phys. Rev. E **92**, 062207 (2015).

[14] D. J. Koeze, D. Vågberg, B. B. T. Tjoa, and B. P. Tighe, Mapping the jamming transition of bidisperse mixtures, Europhys. Lett. **113**, 54001 (2016).

[15] M. Dijkstra, R. van Roij, and R. Evans, Phase Behavior and Structure of Binary Hard-Sphere Mixtures, Phys. Rev. Lett. **81**, 2268 (1998).

[16] J. K. Kummerfeld, T. S. Hudson, and P. Harrowell, The densest packing of AB binary hard-sphere homogeneous compounds across all size ratios, J. Phys. Chem. B **112**, 10773 (2008).

[17] N. Epstein and M. J. Young, Random loose packing of binary mixtures of spheres, Nature (London) **196**, 885 (1962).

[18] D. Pinson, R. P. Zou, A. B. Yu, P. Zulli, and M. J. McCarthy, Coordination number of binary mixtures of spheres, J. Phys. D **31**, 457 (1998).

[19] I. Biazzo, F. Caltagirone, G. Parisi, and F. Zamponi, Theory of Amorphous Packings of Binary Mixtures of Hard Spheres, Phys. Rev. Lett. **102**, 195701 (2009).

[20] L. Meng, P. Lu, and S. Li, Packing properties of binary mixtures in disordered sphere systems, Particuology **16**, 155 (2014).

[21] N. Kumar, V. Magnanimo, M. Ramaioli, and S. Luding, Tuning the bulk properties of bidisperse granular mixtures by small amount of fines, Powder Technol. **293**, 94 (2016).

[22] A. Rosato, K. J. Strandburg, F. Prinz, and R. H. Swendsen, Why the Brazil Nuts are on Top: Size Segregation of Particulate Matter by Shaking, Phys. Rev. Lett. **58**, 1038 (1987).

[23] J. B. Knight, H. M. Jaeger, and S. R. Nagel, Vibration-Induced Size Separation in Granular Media: The Convection Connection, Phys. Rev. Lett. **70**, 3728 (1993).

[24] A. Kudrolli, Size separation in vibrated granular matter, Rep. Prog. Phys. **67**, 209 (2004).

[25] M. Schröter, S. Ulrich, J. Kreft, J. B. Swift, and H. L. Swinney, Mechanisms in the size segregation of a binary granular mixture, Phys. Rev. E **74**, 011307 (2006).

[26] V. Garzó, Thermal diffusion segregation in granular binary mixtures described by the Enskog equation, New J. Phys. **13**, 055020 (2011).
[27] J. J. Brey, N. Khalil, and J. W. Dufty, Thermal segregation beyond Navier-Stokes, New J. Phys. **13**, 055019 (2011).
[28] J. M. Ottino and D. V. Khakhar, Mixing and segregation of granular materials, Annu. Rev. Fluid Mech. **32**, 55 (2000).
[29] F. J. Muzzio, T. Shinbrot, and B. J. Glasser, Powder technology in the pharmaceutical industry: The need to catch up fast, Powder Technol. **124**, 1 (2002).
[30] L.-S. Lu and S.-S. Hsiau, Mixing in vibrated granular beds with the effect of electrostatic force, Powder Technol. **160**, 170 (2005).
[31] Y. Cheng, L. Lee, W. Zhang, and C.-H. Wang, Investigation on electrostatic charging and its effect on mixing of binary particles in a vibrating bed, Ind. Eng. Chem. Res. **53**, 14166 (2014).
[32] W. R. Harper, The generation of static charge, Adv. Phys. **6**, 365 (1957).
[33] L. S. McCarty and G. M. Whitesides, Electrostatic charging due to separation of ions at interfaces: Contact electrification of ionic electrets, Angew. Chem., Int. Ed. **47**, 2188 (2008).
[34] A. Mehrotra, F. J. Muzzio, and T. Shinbrot, Spontaneous Separation of Charged Grains, Phys. Rev. Lett. **99**, 058001 (2007).
[35] S. Chen, W. Liu, and S. Li, Effect of long-range electrostatic repulsion on pore clogging during microfiltration, Phys. Rev. E **94**, 063108 (2016).
[36] A. Schella, S. Herminghaus, and M. Schröter, Influence of humidity on tribo-electric charging and segregation in shaken granular media, Soft Matter **13**, 394 (2017).
[37] S. Nieh and T. Nguyen, Effects of humidity, conveying velocity, and particle size on electrostatic charges of glass beads in a gaseous suspension flow, J. Electrost. **21**, 99 (1988).
[38] S. Pence, V. J. Novotny, and A. F. Diaz, Effect of surface moisture on contact charge of polymers containing ions, Langmuir **10**, 592 (1994).
[39] W. D. Greason, Investigation of a test methodology for triboelectrification, J. Electrost. **49**, 245 (2000).
[40] M. Rhodes, S. Takeuchi, K. Liffman, and K. Muniandy, The role of interstitial gas in the Brazil nut effect, Granular Matter **5**, 107 (2003).
[41] E. Németh, V. Albrecht, G. Schubert, and F. Simon, Polymer tribo-electric charging: Dependence on thermodynamic surface properties and relative humidity, J. Electrost. **58**, 3 (2003).
[42] N. Vandewalle, G. Lumay, F. Ludewig, and J. E. Fiscina, How relative humidity affects random packing experiments, Phys. Rev. E **85**, 031309 (2012).
[43] L. Xie, N. Bao, Y. Jiang, and J. Zhou, Effect of humidity on contact electrification due to collision between spherical particles, AIP Adv. **6**, 035117 (2016).
[44] R. Cademartiri, C. A. Stan, V. M. Tran, E. Wu, L. Friar, D. Vulis, L. W. Clark, S. Tricard, and G. M. Whitesides, A simple two-dimensional model system to study electrostatic-self-assembly, Soft Matter **8**, 9771 (2012).
[45] L. Zitzler, S. Herminghaus, and F. Mugele, Capillary forces in tapping mode atomic force microscopy, Phys. Rev. B **66**, 155436 (2002).
[46] D. Y. Kwok and A. W. Neumann, Contact angle measurement and contact angle interpretation, Adv. Colloid Interface Sci. **81**, 167 (1999).
[47] A. Samadani and A. Kudrolli, Segregation Transitions in Wet Granular Matter, Phys. Rev. Lett. **85**, 5102 (2000).
[48] D. Geromichalos, M. M. Kohonen, F. Mugele, and S. Herminghaus, Mixing and Condensation in a Wet Granular Medium, Phys. Rev. Lett. **90**, 168702 (2003).
[49] W. Hu, L. Xie, and X. Zheng, Contact charging of silica glass particles in a single collision, Appl. Phys. Lett. **101**, 114107 (2012).
[50] L. Xie, G. Li, N. Bao, and J. Zhou, Contact electrification by collision of homogenous particles, J. Appl. Phys. **113**, 184908 (2013).
[51] S. R. Waitukaitis, V. Lee, J. M. Pierson, S. L. Forman, and H. M. Jaeger, Size-Dependent Same-Material Tribocharging in Insulating Grains, Phys. Rev. Lett. **112**, 218001 (2014).
[52] J. F. Kok and D. J. Lacks, Electrification of granular systems of identical insulators, Phys. Rev. E **79**, 051304 (2009).
[53] D. J. Lacks and R. Mohan Sankaran, Contact electrification of insulating materials, J. Phys. D **44**, 453001 (2011).
[54] J. Lowell and W. S. Truscott, Triboelectrification of identical insulators. I. An experimental investigation, J. Phys. D **19**, 1273 (1986).
[55] J. Lowell and W. S. Truscott, Triboelectrification of identical insulators. II. Theory and further experiments, J. Phys. D **19**, 1281 (1986).
[56] G. K. Kaufman, S. W. Thomas III, M. Reches, B. F. Shaw, J. Feng, and G. M. Whitesides, Phase separation of 2D meso-scale Coulombic crystals from meso-scale polarizable “solvent,” Soft Matter **5**, 1188 (2009).
[57] D. Kumar, A. Sane, S. Gohil, P. R. Bandaru, S. Bhattacharya, and S. Ghosh, Spreading of triboelectrically charged granular matter, Sci. Rep. **4**, 5275 (2014).
[58] T. Aste, M. Saadatfar, and T. J. Senden, Geometrical structure of disordered sphere packings, Phys. Rev. E **71**, 061302 (2005).
[59] F. M. Schaller, M. Neudecker, M. Saadatfar, G. Delaney, K. Mecke, G. E. Schröder-Turk, and M. Schröter, Tomographic analysis of jammed ellipsoid packings, in *Powders and Grains 2013: Proceedings of the 7th International Conference on Micromechanics of Granular Media*, edited by A. Yu, K. Dong, R. Yang, and S. Luding, AIP Conf. Proc. Vol. 1542 (AIP, Melville, NY, 2013), pp. 377–380.
[60] S. Weis and M. Schröter, Analyzing X-ray tomographies of granular packings, Rev. Sci. Instrum. **88**, 051809 (2017).
[61] G. E. Schröder-Turk, W. Mickel, M. Schröter, G. W. Delaney, M. Saadatfar, T. J. Senden, K. Mecke, and T. Aste, Disordered spherical bead packs are anisotropic, Europhys. Lett. **90**, 34001 (2010).
[62] K. Barros and E. Luijten, Dielectric Effects in the Self-Assembly of Binary Colloidal Aggregates, Phys. Rev. Lett. **113**, 017801 (2014).
[63] F. M. Schaller, M. Neudecker, M. Saadatfar, G. W. Delaney, G. E. Schröder-Turk, and M. Schröter, Local Origin of Global Contact Numbers in Frictional Ellipsoid Packings, Phys. Rev. Lett. **114**, 158001 (2015).